

RESEARCH ARTICLE

Tunable broadband photoluminescence from bismuth-doped calcium aluminum germanate glasses prepared in oxidizing atmosphere

Jiangkun Cao  | Yicong Ding  | René Limbach  | Vahid Nozari | Roman Sajzew | Minghui Sun | Pengzhu Zhang | Lothar Wondraczek 

Otto Schott Institute of Materials
Research, Friedrich Schiller University
Jena, Jena, Germany

Correspondence

Jiangkun Cao, Otto Schott Institute of
Materials Research, Friedrich Schiller
University Jena, Fraunhoferstrasse 6,
07743 Jena, Germany.
Email: jiangkun.cao@uni-jena.de

Funding information

European Research Council,
Grant/Award Number: 681652

Abstract

Tunable photoluminescence (PL) from transparent inorganic glass matrices is of interest for applications demanding a semitransparent photoconverter that does not elastically scatter incoming light. For this purpose, bismuth (Bi)-doped optical materials exhibit unique spectral characteristics in terms of bandwidth and emission tunability. Here, we demonstrate a facile route for preparing such converters from Bi-doped calcium-aluminate and calcium-aluminogermanate glasses. These glasses offer tunable PL across the near violet and visible-to-near-infrared (NIR) spectral range, with an emission lifetime in the range of 300 μ s. The addition of GeO₂ exerts a decrease in optical basicity, which in turn enables the stabilization of NIR-active low-valence Bi species for broadband NIR PL.

KEYWORDS

bismuth, broadband, glass, NIR, photoluminescence

1 | INTRODUCTION

Materials that exhibit tunable and broadband photoluminescence (PL) are of great interest for customized visible-to-infrared light sources and spectral converters, for example, for highly sensitive temperature sensing, high-density optical communication, photodynamic therapy, or photochemical energy conversion.^{1–6} Such converter materials rely on the combination of a robust matrix phase with one or more suitable activator species. When glasses are used for this purpose, the activator can be homogeneously incorporated into the material, which avoids light scattering at particle–matrix interfaces. In addition, the

full range of glass processing technology is—in principle—available for generating materials of the desired shapes and sizes. Furthermore, glass matrices offer highest compositional flexibility, from activator solubility to redox control and the tailoring of secondary properties (e.g., mechanical, chemical, or optical).^{7,8} Diverse light sources ranging from ultraviolet (UV) to infrared PL have been achieved with glasses, mostly using f–d or f–f electronic transitions in rare-earth (RE) dopants.^{9–11} The 4f electrons of the various RE species are fully shielded by the 5s² and 5p⁶ electrons, which results in limited tunability of the PL characteristics of f–f transitions when exposed to variable glass chemical environments (with only some of the degenerate states

This is an open access article under the terms of the [Creative Commons Attribution-NonCommercial-NoDerivs](https://creativecommons.org/licenses/by-nc-nd/4.0/) License, which permits use and distribution in any medium, provided the original work is properly cited, the use is non-commercial and no modifications or adaptations are made.

© 2022 The Authors. *Journal of the American Ceramic Society* published by Wiley Periodicals LLC on behalf of American Ceramic Society.

depending on ligand symmetry and orbital distortion).¹² Therefore, alternative activator species are of interest beyond the REs for achieving broadband PL.

Transition metal ions with their weakly bound d electrons (such as V^{5+} , Ti^{4+} , Cu^{+} , Mn^{2+} , Cr^{4+} , Co^{2+} , Ni^{2+} , and Ag^{+}),^{13–21} main group metal ions (such as Pb^{+} , Sn^{2+} , Bi^{3+} , Te^{4+} , and Sb^{3+}),^{22–28} quantum dots (such as PbS^{29}), and structural defects (such as oxygen vacancies³⁰) present such alternatives. Among these, bismuth (Bi) ions are of particular interest due to their large variability in terms of the oxidation state that can be stabilized in glass matrices.²³ This has enabled Bi-activated optical materials with PL ranging from the UV to the near-infrared (NIR) and mid-infrared spectral region.^{6,31–35} In particular, Bi-doped glasses and fibers are considered active gain media with broadband and tunable NIR emission.^{36–38}

The PL characteristics of Bi embedded in glass are highly sensitive to redox conditions, doping concentration, and local environment. Although this is problematic when targeting materials with well-defined, homogeneous properties, it simultaneously offers a multitude of opportunities for tailoring the PL performance. These include variations in melting time and temperature,³⁹ melting atmosphere,³⁸ post-processing,^{40,41} or interactions with external stimuli (such as laser or gamma-ray irradiation).^{42–44} Aside these parameters, tailoring the chemical composition of the matrix glass is the primary way of modulating bismuth speciation; a range of glass types have been studied as host materials for optically active bismuth species.^{45–51} In particular, Bi-doped germanium-containing glasses and fibers have been identified as candidate materials with unique NIR emission behavior, especially in the important C-band spectral region. The characteristic properties of these glasses are presumably originating from interactions of active Bi species with germanium-related oxygen deficiency.⁵² Although some progress has recently been made in the exploitation of such novel broadband light sources, further insight on the optical behavior of Bi active ions as a function of systematic variations in the chemistry of these glasses and, in particular, their preparation in air atmosphere is still lacking.

Efficient broadband visible emission was previously observed from Bi-activated aluminate glasses, induced by local network basicity.⁵³ The emission spectrum was found to cover the whole visible range. Here, we now consider the systematic introduction of GeO_2 as a network-forming species into calcium-aluminate glasses as a means to tailor the mechanical and the PL characteristics of Bi-doped aluminate glasses. As an important feature, these glasses are produced in air atmosphere so as to enable facile forming or post-processing.

2 | EXPERIMENTAL SECTION

2.1 | Sample preparation

Bulk glass samples with nominal compositions of $(100 - x)[0.63CaO - 0.37Al_2O_3] - xGeO_2 - 0.25Bi_2O_3$ ($x = 0, 10, 30, 40, 60, 80, 90,$ and 100 mol%) were prepared by conventional melt-quenching in air. Batches (~ 40 g) of analytical grade reagents of GeO_2 , Al_2O_3 , $CaCO_3$, and Bi_2O_3 (Sinopharm Chemical Reagent Co., Ltd.) were weighted in powder form, mixed, and melted in alumina crucibles at $1500^\circ C$ for 30 min in air. Then, the melt was poured onto a preheated ($\sim 200^\circ C$) stainless-steel plate and pressed with another plate to form bulk glass samples (denoted as xGe , where x refers to the nominal GeO_2 concentration in mol%). Quenched bulk samples were cut and polished in coplanar geometry to optical grade for further characterization, using a CeO_2 suspension as the polishing agent. The specimen size was about $2 \times 10 \times 15$ mm³. Sample 100Ge was visually transparent, but notably hygroscopic, which is why it was excluded from the analyses in this study.

2.2 | Glass characterization

X-ray diffraction (XRD) patterns were collected on a powder diffractometer (Miniflex 600) over the angular range of $10^\circ \leq 2\theta \leq 80^\circ$ using $Cu K_\alpha$ radiation (step size: 0.01°). The glass transition temperature T_g , onset of crystallization T_x , and peak temperature of crystallization T_p were obtained by differential scanning calorimetry (DSC, Netzsch STA 449 F3 Jupiter) in a Pt crucible under flowing N_2 at a heating rate of 10 K/min. The glass density ρ was determined via Archimedes' principle at $20^\circ C$ using ethanol as the immersion liquid. Molar volumes V_m are obtained by $V_m = M/\rho$. M denotes the average molar mass of the glass that is calculated from the molar masses of individual glass components and the glass composition. Elastic properties were calculated from transversal and longitudinal sound velocities, v_L and v_T , respectively,⁵⁴ as determined by ultrasonic echography using piezoelectric transducers operating at frequencies of 8–12 MHz (Echometer 1077, Karl Deutsch). Raman spectra were collected with a dispersive confocal Raman microscope (Renishaw inVia) for wavenumbers ranging from 80 to 1000 cm^{-1} at step widths of 1.5 cm^{-1} , using the 514-nm excitation line of an Ar-laser. Fourier transform infrared spectroscopy (FTIR) spectra were collected in a Perkin Elmer FTIR spectrometer in reflection mode (450 – 1050 cm^{-1}) at step widths of 2 cm^{-1} . Each spectrum was averaged over 10 consecutive scans. The room temperature visible (Vis) and

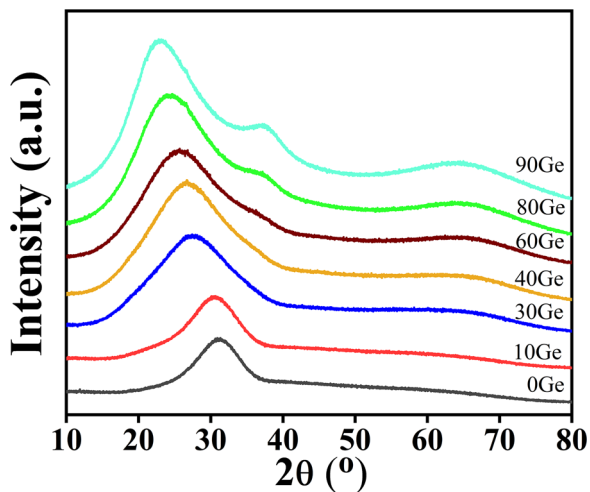


FIGURE 1 XRD patterns of the $(100 - x)[0.63\text{CaO}-0.37\text{Al}_2\text{O}_3] - x\text{GeO}_2-0.25\text{Bi}_2\text{O}_3$ glasses (denoted as $x\text{Ge}$, with $x = 0, 10, 30, 40, 60, 80,$ and 90 mol%). XRD, X-ray diffraction

NIR emission and excitation spectra were measured with a high-resolution spectrofluorometer (Fluorolog-3, Horiba JobinYvon) using a continuous wave 450-W Xe-lamp as a pump source and a Hamamatsu R2658P (UV-Vis spectral range) or H10330 PMT (NIR spectral range) photomultiplier tube, respectively, as a detector. Photographs of the samples under both sunlight and 365-nm LED irradiation were recorded with a digital camera (Canon EOS 850D). The decay curves were measured using an FLS920 spectrofluorometer (Edinburgh Instruments) equipped with a microsecond flashlamp (μF900) as an excitation source. Optical transmittance spectra were recorded on a dual-beam spectrophotometer (Cary 5000, Agilent) in the spectral range of 200–2000 nm at step widths of 2 nm. Optical basicity was calculated according to references.^{55,56}

3 | RESULTS AND DISCUSSION

Figure 1 shows the XRD patterns of melt-quenched samples with a nominal composition of $(100 - x)[0.63\text{CaO}-0.37\text{Al}_2\text{O}_3] - x\text{GeO}_2-0.25\text{Bi}_2\text{O}_3$ ($x = 0, 10, 20, 30, 40, 60, 80,$ and 90 , denoted as 0Ge, 10Ge, 30Ge, 40Ge, 60Ge, 80Ge, and 90Ge, respectively). All samples exhibit a broad diffraction maximum with no visible sign for crystallinity across the whole range of GeO_2 substitution.

DSC up-scans of the $x\text{Ge}$ glasses are presented in Figure 2A. The values of T_g , T_x , and T_p are listed in Table 1. For clarity, the DSC curve of the 90GeO₂ sample is provided individually in Figure 2B. The addition of increasing amounts of GeO_2 to the calcium-aluminate-based glass causes a significant drop in T_g , that is, from ~ 838 (0Ge) to $\sim 604^\circ\text{C}$ (90Ge), whereas T_x is decreasing less strongly, from ~ 904 (0Ge) to $\sim 829^\circ\text{C}$ (90Ge). In turn, this results in a gradual expansion of the supercooling range as a function of the GeO_2 concentration, from $\sim 70^\circ\text{C}$ (0Ge) to $\sim 225^\circ\text{C}$ (90Ge).

With the addition of GeO_2 (with a higher molecular weight of 104.64 g/mol, relative to Al_2O_3 [101.96 g/mol] and CaO [56.08 g/mol]), the mass density of the glasses gradually increases from ~ 2.91 g/cm³ for the GeO_2 -free glass to ~ 3.63 g/cm³ for 40 mol% GeO_2 ; for higher degrees of substitution, only minor changes in mass density are observed (Figure 3A). The opposite trends are seen for the sound wave velocities and elastic properties. Both the values of v_L and v_T are decreasing monotonically with the progressive increase in the GeO_2 concentration (Figure 3B). Likewise, the shear modulus G , bulk modulus K , and Young's modulus E are decreasing (Figure 3C). This decrease in mechanical performance is supposed to be a direct consequence of the gradual decrease in the bond energy density (expressed as the dissociation energy per unit volume G_i), when

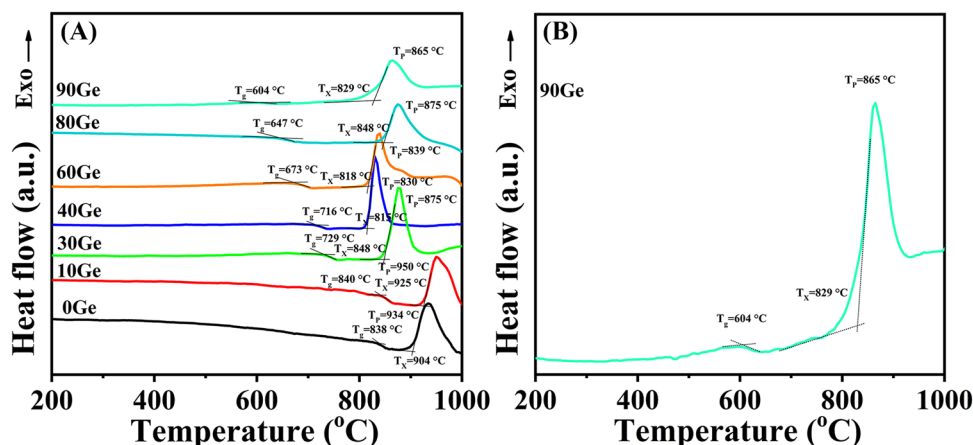


FIGURE 2 (A) DSC curves of the $(100 - x)[0.63\text{CaO}-0.37\text{Al}_2\text{O}_3] - x\text{GeO}_2-0.25\text{Bi}_2\text{O}_3$ glasses (denoted as $x\text{Ge}$, with $x = 0, 10, 30, 40, 60, 80,$ and 90 mol%). Characteristic temperatures, including the glass transition temperature T_g , onset of crystallization T_x , and peak temperature of crystallization T_p , are indicated by the labels. (B) Individual DSC curve of the 90Ge sample. DSC, differential scanning calorimetry

TABLE 1 Mechanical and optical properties of x Ge glasses: Transition temperature (T_g), onset crystallization temperature (T_x), peak crystallization temperature (T_p), mass density (ρ), optical basicity (Λ), molar volume (V_m), longitudinal modulus (L), shear modulus (G), bulk modulus (K), Young's modulus (E), and Poisson's ratio (ν)

	Thermal properties				P (g/cm ³)	Λ	V_m (cm ³ /mol)	L (GPa)	G (GPa)	K (GPa)	E (GPa)	ν
	T_g	T_x	T_p	ΔT								
0Ge	834	904	934	70	2.91	0.745	25.47	139.7	41.8	83.9	107.6	0.286
10Ge	840	925	950	85	3.04	0.730	25.43	133.6	40.2	80.1	103.3	0.285
30Ge	729	848	875	119	3.52	0.700	23.76	111.3	33.7	66.5	86.4	0.283
40Ge	716	815	830	99	3.63	0.686	23.90	105.5	32.0	62.8	82.2	0.282
60Ge	673	818	839	145	3.67	0.659	25.39	93.5	29.7	53.9	75.3	0.267
80Ge	647	848	875	201	3.67	0.634	27.10	80.0	26.6	44.5	66.6	0.251
90Ge	604	829	865	225	3.65	0.621	28.12	62.3	21.8	33.2	53.7	0.230
100Ge	~550 ⁵⁸	–	–	–	3.63 ⁵⁹	0.610	29.15	48.0 ⁵⁹	18.1 ⁵⁹	23.9 ⁵⁹	43.3 ⁵⁹	0.197

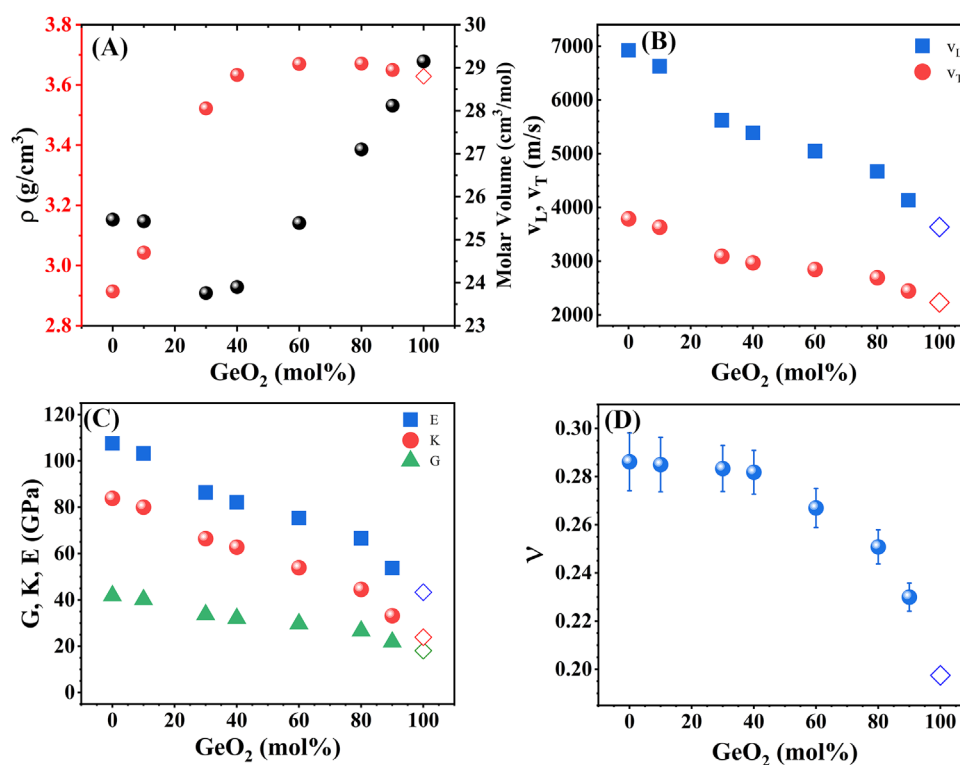


FIGURE 3 Compositional dependence of (A) density ρ and molar volume V_m , (B) longitudinal v_L and transversal v_T sound wave velocities, (C) shear modulus G , bulk modulus K , and Young's modulus E , and (D) Poisson's ratio ν of $(100 - x)$ $[0.63\text{CaO}-0.37\text{Al}_2\text{O}_3] - x\text{GeO}_2-0.25\text{Bi}_2\text{O}_3$ glasses on the GeO_2 content. Available literature data for pure vitreous GeO_2 (100Ge) is added for comparison (open diamond in panels (A)–(D))^{58,59}

Al–O ($G_i = 119.2 \text{ kJ/cm}^3$) is replaced by increasing amounts of Ge–O ($G_i = 49.5 \text{ kJ/cm}^3$).⁵⁷ Interestingly, Poisson's ratio ν (Figure 3D) remains almost invariant at around 0.28 for moderate amounts of up to 40 mol% GeO_2 ($\nu = 0.286$ for 0Ge, as compared to $\nu = 0.282$ for 40Ge) but then suddenly decreases down to 0.230 (90Ge). The molar volume V_M tends to decrease first but then increases with the further addition of GeO_2 . Table 1 summarizes the experimentally

determined thermal, mechanical, and optical parameters of the studied x Ge glasses.

Raman (Figure 4A,B) and FTIR (Figure 4C) spectra were recorded to monitor the structural variations induced by the addition of increasing amounts of GeO_2 to the calcium-aluminate glasses. For clarity, two selected Raman spectra (0Ge and 90Ge) are highlighted individually in Figure 4B. The Raman spectrum for GeO_2 -free

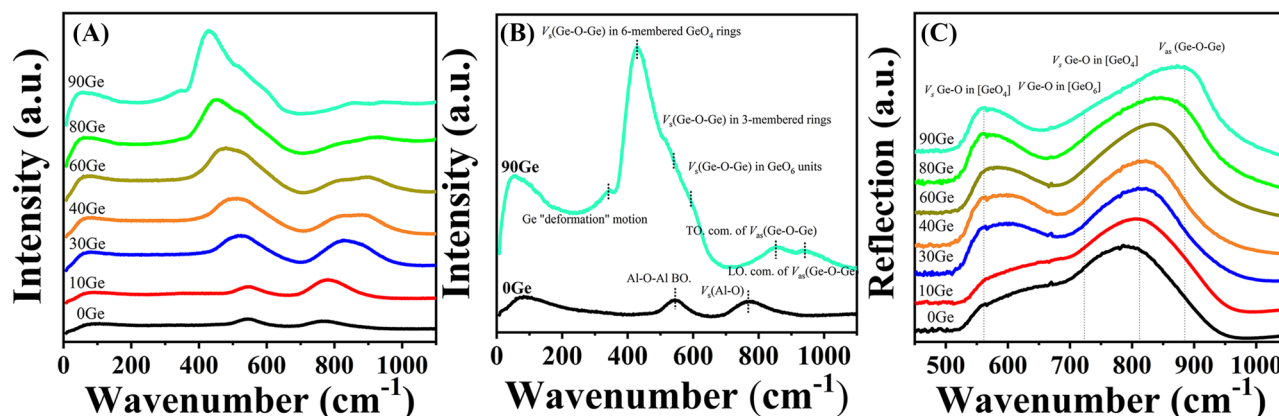


FIGURE 4 (A) Raman scattering spectra of the $(100 - x)[0.63\text{CaO} - 0.37\text{Al}_2\text{O}_3] - x\text{GeO}_2 - 0.25\text{Bi}_2\text{O}_3$ glasses (denoted as $x\text{Ge}$, with $x = 0, 10, 30, 40, 60, 80,$ and 90 mol%). (B) Raman spectra of the 0Ge and 90Ge glasses with the respective band assignments. (C) FTIR reflection spectra. FTIR, Fourier transform infrared spectroscopy

calcium-aluminate glasses (0Ge) exhibits two main vibration bands located at 545 and 770 cm^{-1} . Without aiming to go into details at this point, the band at 545 cm^{-1} is related to motions of bridging oxygen ions within the $\text{Al}-\text{O}-\text{Al}$ linkages, whereas the high-frequency band at 770 cm^{-1} is due to aluminum-oxygen stretching vibrations of the fully polymerized tetrahedral aluminate groups.^{60–62} The Raman spectrum of the GeO_2 -rich glass (90Ge) exhibits a strong peak located at 426 cm^{-1} with three shoulders at ~ 347 , ~ 540 , and $\sim 580\text{ cm}^{-1}$. The 347 cm^{-1} vibration results from Ge deformation modes within the glass network, and the 426 cm^{-1} vibration is attributed to the symmetric stretching of $\text{Ge}-\text{O}-\text{Ge}$ in GeO_4 six-membered rings.⁶³ The 540 cm^{-1} feature is assigned to the symmetric breathing mode of $\text{Ge}-\text{O}-\text{Ge}$ in smaller GeO_4 rings, or AlO_4 breathing modes. The shoulder at 580 cm^{-1} may originate from the stretching vibrations of $\text{Ge}-\text{O}-\text{Ge}$ in GeO_6 units.⁶⁴ Besides the dominant band located at 426 cm^{-1} , two weaker bands were detected at 820 and 900 cm^{-1} . We assign these to the transverse and longitudinal split components, respectively, of the asymmetric stretching of $\text{Ge}-\text{O}-\text{Ge}$ bonds.⁶⁵ Compared to Bi-doped aluminate glasses, with an increase in GeO_2 content, new peaks located at 500 , 820 , and 900 cm^{-1} emerged, indicating the formation of $\text{Ge}-\text{O}-\text{Ge}$ in small GeO_4 rings. With increasing GeO_2 content, the band at 500 cm^{-1} shifts to lower frequency, indicating the formation of larger rings. At the same time, the bands located at 820 and 900 cm^{-1} shift to higher frequency, which indicates a reduction of the fraction of non-bridging oxygen ions.⁶⁶ The FTIR spectra exhibit a broadband envelope spanning the spectral range between 500 and 1000 cm^{-1} . These bands cannot be assigned accurately to either $\text{Ge}-\text{O}-\text{Ge}$ of GeO_4 or $\text{Al}-\text{O}$ of AlO_4 or AlO_6 , due to strong overlap between all modes. The $570\text{--}600\text{ cm}^{-1}$ and the $720\text{--}815\text{ cm}^{-1}$ regions are ascribed to the $\text{Ge}-\text{O}$ stretching vibrations of GeO_4

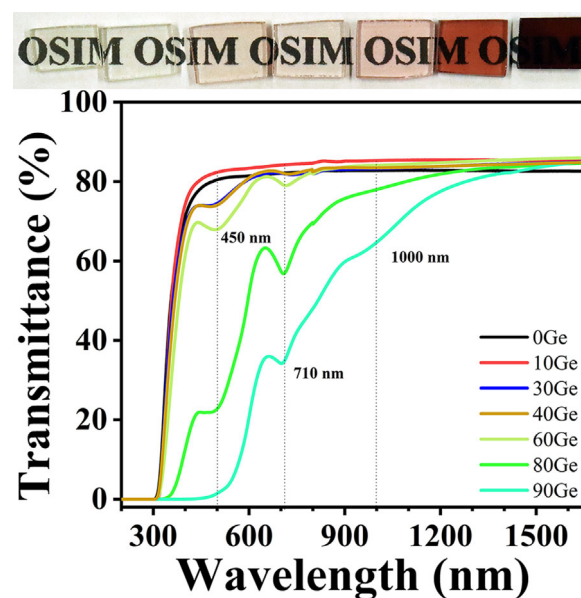


FIGURE 5 UV-Vis-NIR optical transmittance spectra of Bi-doped glass with different GeO_2 concentrations (for a specimen thickness of 2 mm). The inset shows sample photographs, with GeO_2 content increasing from left to right. NIR, near-infrared; UV, ultraviolet; Vis, visible

tetrahedral units.⁶⁶ $\text{Ge}-\text{O}$ vibrations in GeO_6 structural units occur around 690 cm^{-1} .⁶⁷ The peak near 880 cm^{-1} may reflect the asymmetric stretching vibration of $\text{Ge}-\text{O}-\text{Ge}$ bridges shifting to higher frequency with increasing in GeO_2 content. The latter indicates a coordination change from GeO_4 to GeO_6 .⁶⁸

UV-Vis-NIR transmittance spectra of the Bi-doped glass samples are shown in Figure 5. The pure Bi-doped calcium-aluminate glass (0Ge) is highly transparent from the near UV to the NIR spectral region and does not exhibit any pronounced absorption band over the full visible spectral

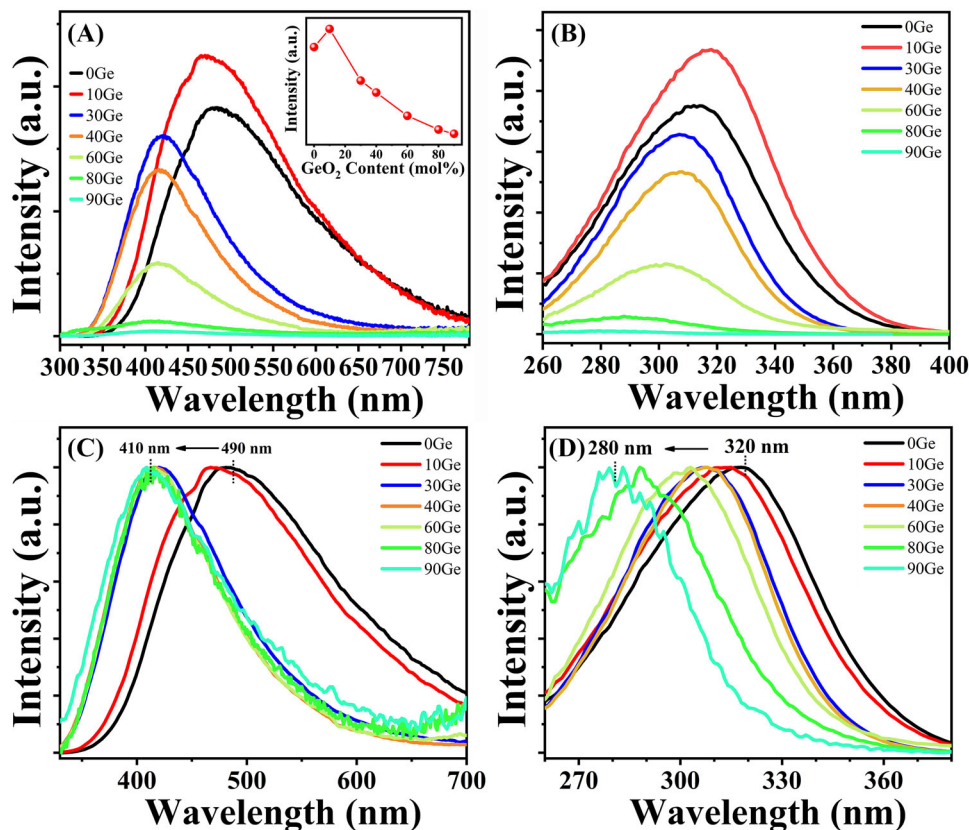


FIGURE 6 (A) Visible photoluminescence spectra of the $(100 - x)[0.63\text{CaO}-0.37\text{Al}_2\text{O}_3] - x\text{GeO}_2-0.25\text{Bi}_2\text{O}_3$ glasses (denoted as $x\text{Ge}$, with $x = 0, 10, 30, 40, 60, 80,$ and 90 mol%) excited by the corresponding maximum excitation wavelength for each sample. The inset depicts the visible photoluminescence intensity integrated over the spectral range of $300\text{--}790$ nm as a function of the GeO_2 content. (B) Photoexcitation spectra obtained by monitoring the emission bands in (A). (C) Normalized photoluminescence spectra of the studied glasses excited by UV light. (D) Normalized photoexcitation spectra corresponding to panel (B). UV, ultraviolet

range. This significantly changes upon the introduction of GeO_2 . For low contents of GeO_2 (10Ge), glasses are still highly transparent (up to 80% transmittance at 550 nm) and the spectra remain mostly flat in the Vis–NIR region. With further increase in GeO_2 content (from 30Ge to 90Ge), a notable red-shift of the absorption edge occurs, and various characteristic absorption bands emerge in the spectral range of $300\text{--}1200$ nm. As a result, the samples gradually change from colorless to pink and, eventually, dark red (inset of Figure 5). The absorption bands are characteristic for bismuth doped into glass matrices; however, their specific assignment remains ambiguous; bismuth speciation and the origin of Bi-related NIR emission in glasses are still under debate.^{23,33} Noteworthy, the absorption bands (located at 450, 710, and 1000 nm) do not shift as a function of GeO_2 content.

The changes in the spectral transmission are well reflected in the PL characteristics of the glasses with increasing GeO_2 content. Under UV excitation, as presented in Figure 6A, a broad PL band centered at ~ 500 nm was observed in samples 0Ge and 10Ge. This band covers the near violet and Vis–NIR region. As demonstrated

in a previous work, Bi^{2+} presents red-to-NIR emission in polycrystals with different emission and excitation features compared to Bi^{3+} and Bi^+ .⁶⁹ It is possible that Bi^{2+} also exists in these glasses, but we did not observe the characteristic optical properties of that species. Thus, Bi^{2+} may exist as nonluminescent centers in the glasses discussed in this study. In addition, the lifetime of Bi^{3+} in crystals is normally in the range of $10^{-5}\text{--}10^{-8}$ s. In our previous report, we observed a lifetime of ~ 1 μs in Bi-doped aluminate glasses, which is in the same order of magnitude as the luminescence lifetime of bismuth in germanate glasses and phosphors, especially for aluminate phosphors.^{70–72} Thus, we tend to attribute this emission to the $^3\text{P}_1 \rightarrow ^1\text{S}_0$ transition in Bi^{3+} .⁷³ With the introduction of higher amounts of GeO_2 , the emission intensity of this band continuously decreases, which is accompanied by a blue-shift from about 490 to 410 nm, as seen in Figure 6C. The integrated emission intensity is decreased by ~ 50 times for 90Ge as compared to that of 0Ge (the inset of Figure 6A). Analogous to the PL spectra, a broad excitation band was detected for $^1\text{S}_0 \rightarrow ^3\text{P}_1$ of Bi^{3+} ,⁷⁴ shown in Figure 6B. With increasing GeO_2 content, this band, too,

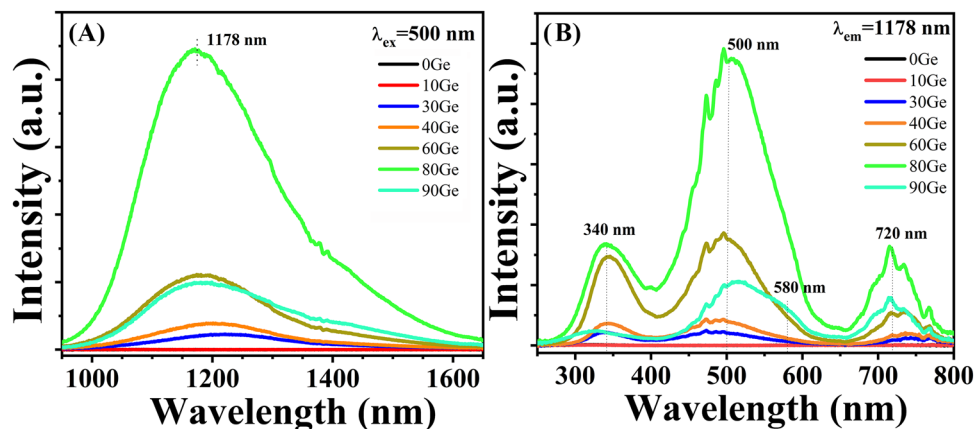


FIGURE 7 (A) Emission spectra ($\lambda_{\text{ex}} = 500 \text{ nm}$) of the $(100 - x)[0.63\text{CaO}-0.37\text{Al}_2\text{O}_3] - x\text{GeO}_2-0.25\text{Bi}_2\text{O}_3$ glasses (denoted as $x\text{Ge}$, with $x = 0, 10, 30, 40, 60, 80$, and 90 mol\%). (B) Excitation spectra for emission from the studied glasses at 1178 nm

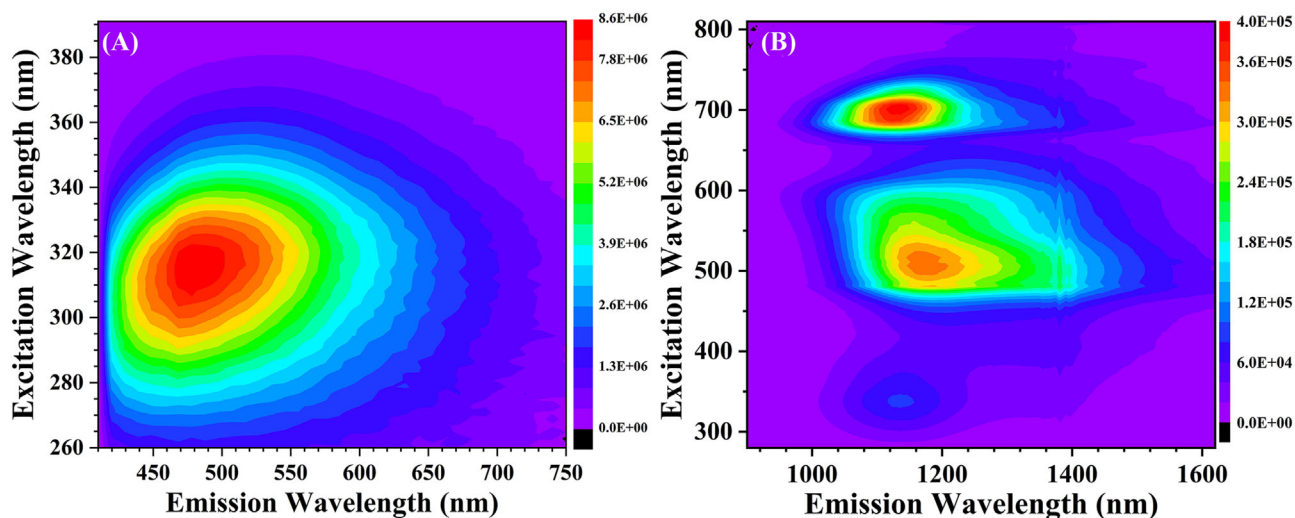


FIGURE 8 Contour plots of the NIR emission intensity (color code) as a function of excitation and emission wavelength for the (A) 10Ge sample and (B) 90Ge sample. NIR, near-infrared

decreases in intensity and shifts to shorter wavelength, that is, from 320 to 280 nm (Figure 6D).

Corresponding to the emerging absorption bands in Figure 5, the addition of GeO_2 leads to strong changes in the NIR emission spectra. Notable broadband NIR PL from Bi NIR active centers³³ is detected from sample 30Ge onward, with a maximum excitation efficiency at $\sim 500 \text{ nm}$ and an emission band maximum at $\sim 1178 \text{ nm}$ with a full width at half maximum (FWHM) of $\sim 200 \text{ nm}$.

Obviously, the addition of GeO_2 leads to a reduction of Bi^{3+} in favor of NIR-active Bi centers. A maximum in emission intensity is observed for the 80Ge glass. Assumedly, concentration quenching and self-absorption are set at higher GeO_2 content, for which samples become increasingly absorbing in the spectral range of excitation as well as emission (Figure 6). The FWHM of the NIR emis-

TABLE 2 CIE color coordinates of sample 10Ge with different excitation wavelength

	285 nm	300 nm	315 nm	330 nm	345 nm	360 nm	375 nm
CIE x	0.27	0.27	0.28	0.30	0.31	0.32	0.33
CIE y	0.31	0.32	0.33	0.35	0.37	0.39	0.40

Abbreviation: Commission Internationale de L'clairage.

sion spectra increases from 190 nm (30Ge) to 220 nm (90Ge); for 80Ge and 90Ge samples, emission at the longer wavelengths becomes increasingly important ($\sim 1450 \text{ nm}$), indicating the coexistence of multiple Bi NIR centers, such as Bi^+ and Bi^0 .⁷⁵ It is worth mentioning that, over the last decades, various arguments and models have been proposed, approaching the subject from three main

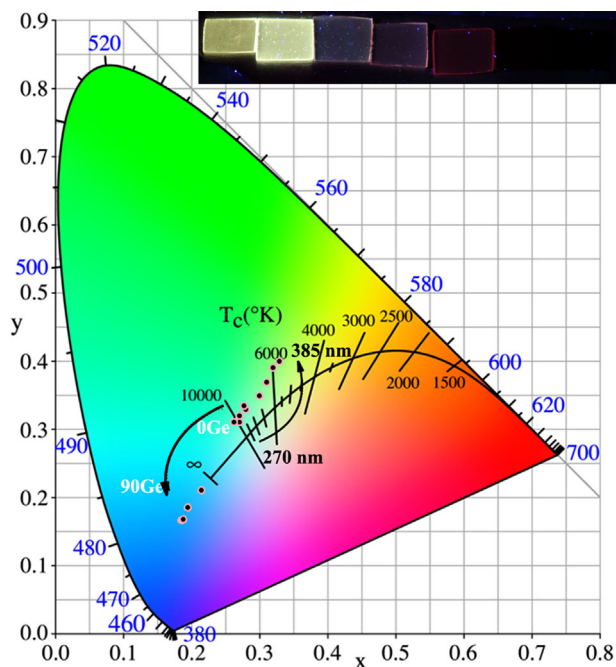


FIGURE 9 CIE chromaticity diagram for photoluminescence from $x\text{Ge}$ samples with gradually increasing GeO_2 content, and the 10Ge sample while varying the excitation wavelength from 270 to 385 nm. The inset shows sample images of $x\text{Ge}$ glasses under UV 365 nm excitation. CIE, Commission Internationale de L'clairage; UV, ultraviolet

directions: (i) bismuth in higher valency, that is, Bi^{5+} and related molecules^{76,77}; (ii) bismuth in lower valency, that is, BiO , Bi^+ , Bi^0 , cluster ions^{78–80}; and (iii) point defects of oxygen.⁵² Here, we tend to discuss the results based on (ii). This is also motivated by previous observations in relation to preparation conditions, glass composition, and surrounding environment.^{81,82}

Monitoring the 1178-nm emission line (Figure 7B), no excitation signal was detected in the 0Ge and 10Ge sam-

ples, in which only Bi^{3+} ions are optically active. With increasing GeO_2 content, a broadband excitation feature emerges, with main contributions at about 340, 500, and 720 nm. In good accordance with the emission spectra, also the excitation spectrum reaches its maximum intensity for the 80Ge glass. Furthermore, for 80Ge and 90Ge, a fourth excitation band is detected at ~ 580 nm. This latter observation confirms that multiple Bi NIR active centers coexist in glasses with higher GeO_2 concentrations.

Making use of the coexistence of multiple Bi active centers, the emission of sample 90Ge and sample 10Ge can be widely tuned so as to cover the whole visible and NIR spectral region. Contour plots of the excitation–emission characteristics of 10Ge and 90Ge are provided in Figure 8A,B, respectively. As shown in Figure 8A, the peak for visible emission shifts from blue to green under different excitation conditions; it exhibits a large degree of tunability. The visible emission can be excited by light from deep UV to NIR; it can be accessed by commercial UV LEDs, for example, operating at 365 nm. Correspondingly, the emission spectra cover the whole visible range, offering great potential for broadband illumination tasks. The NIR emission band position in Figure 8B varies from 1100 to 1400 nm under variable excitation wavelength. The emission distribution further highlights the coexistence of multiple Bi NIR active ion species. As the excitation wavelength increases, PL of the 10Ge occurs predominantly at ~ 480 nm. For the 90Ge sample, there are two spectral regions (~ 1200 and ~ 1400 nm, respectively) in the emission spectra, indicating that at least two Bi NIR active centers are created as results of GeO_2 addition.

Accordingly, the emission color changes from green (under 270 nm) to yellow (under 385 nm) when gradually adjusting the excitation wavelength, as shown in Figure 9. The color coordinates of Commission Internationale de L'clairage of the 10Ge sample under different excitations

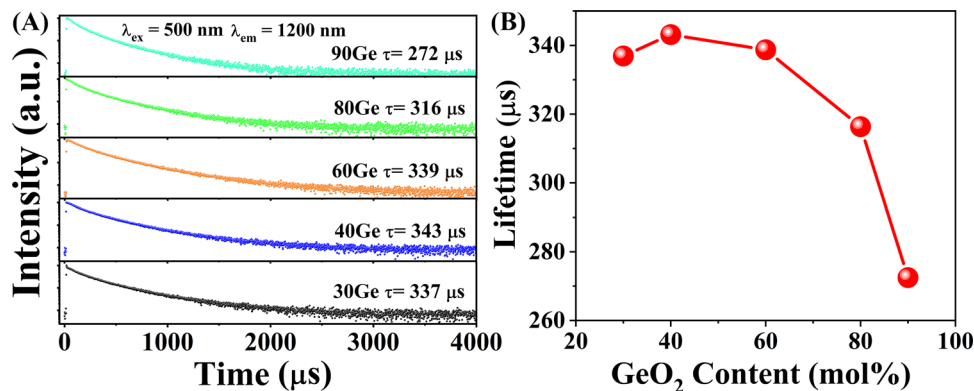


FIGURE 10 (A) NIR photoluminescence decay behavior of Bi NIR active center in the $(100 - x) [0.63\text{CaO}-0.37\text{Al}_2\text{O}_3] - x\text{GeO}_2-0.25\text{Bi}_2\text{O}_3$ glasses (denoted as $x\text{Ge}$, with $x = 30, 40, 60, 80,$ and 90 mol%) for 1200-nm emission excited at 500 nm. (B) The composition-dependent lifetime for $x\text{Ge}$ samples. NIR, near-infrared

are listed in Table 2. In the inset of Figure 9, we further provide sample photographs for xGe under 365 nm UV light irradiation. Besides, with increasing GeO₂ content from 10 to 90 mol%, the emission intensity increases first and then decreases gradually, and the color changes from yellow to red. Noteworthy, 80Ge and 90Ge with high content of GeO₂ present almost no visible PL.

The PL decay data corroborate our previous arguments (Figure 10). Monitoring the 1200-nm emission (Figure 10A) for 30Ge, 40Ge, 60Ge, 80Ge, and 90Ge (e.g., 0Ge and 10Ge, we refrain from measuring decay curves due to the very low NIR emission intensity), we find that the emission lifetime first increases and then decrease, attaining a peak for sample 40Ge (Figure 10B). This is due to the conversion of Bi ions from high to low valence, inducing the concentration quenching of Bi NIR centers. For all decay data, there is a clear deviation from a single-exponential kinetic function: There are multiple Bi NIR active centers or multiple energy relaxation paths responsible for the observed PL characteristics.

When using Bi₂O₃ as a raw material in the preparation of Bi-doped glasses, Bi₂O₃ tends to decompose into Bi atoms and oxygen.⁸³ In Bi-doped aluminate glasses, the high optical basicity hinders this reaction and preserves Bi³⁺ ions with broadband visible PL.⁸⁴ With the addition of GeO₂, the optical basicity is lowered (Table 1), which favors Bi-active species with lower valence. Their interaction with oxygen defects in germanate glasses results in the NIR emission located at 1400 nm.⁸⁵

4 | CONCLUSIONS

In summary, we demonstrated a facile way to modulate Bi visible and NIR emission PL characteristics in multicomponent glasses through adjustments in glass chemistry. Calcium-aluminum-germanate glass matrices enable highly tunable Vis to NIR PL from Bi active centers through adapting the GeO₂ content. Moderate amounts of GeO₂ cause a blue-shift of the visible emission as well as of the excitation bands. At high GeO₂ content, Bi-visible emission is reduced in favor of broadband NIR emission located at 1178 and 1400 nm, due to the reduction of the Bi-active species. Besides, the addition of GeO₂ to the aluminate-based glass leads to a decrease in glass transition temperature and elastic constants.

ACKNOWLEDGMENTS

This project has received funding from the European Research Council (ERC) under the European Union's Horizon 2020 research and innovation program (Grant no. 681652). We would like to thank our colleague Christian Zeidler for technical support with optical spectroscopy.


Open Access funding enabled and organized by Projekt DEAL.

ORCID

Jiangkun Cao  <https://orcid.org/0000-0001-7631-2797>

Yicong Ding  <https://orcid.org/0000-0002-6167-4098>

René Limbach  <https://orcid.org/0000-0002-9716-7178>

Lothar Wondraczek  <https://orcid.org/0000-0002-0747-3076>

REFERENCES

- Xiao Y, Xiao W, Wu D, Guan L, Luo M, Sun LD. An extra-broadband VIS–NIR emitting phosphor toward multifunctional LED applications. *Adv Funct Mater.* 2021;32:2109618.
- Kang Z, Wang S, Seto T, Wang Y. A highly efficient Eu²⁺ excited phosphor with luminescence tunable in visible range and its applications for plant growth. *Adv Opt Mater.* 2021;9:2101173.
- Zheng T, Sójka M, Runowski M, Woźny P, Lis S, Zych E. Tm²⁺ activated SrB₄O₇ bifunctional sensor of temperature and pressure-highly sensitive, multi-parameter luminescence thermometry and manometry. *Adv Opt Mater.* 2021;9:2101507.
- Dianov EM, Semjonov S, Bufetov IA. New generation of optical fibres. *Quantum Electron.* 2016;46(1):1.
- Wondraczek L, Batentschuk M, Schmidt MA, Borchardt R, Scheiner S, Seemann B, et al. Solar spectral conversion for improving the photosynthetic activity in algae reactors. *Nat Commun.* 2013;4(1):1–6.
- Peng M, Wondraczek L. Bismuth-doped oxide glasses as potential solar spectral converters and concentrators. *J Mater Chem.* 2009;19(5):627–30.
- Varshneya AK, Mauro JC., *Fundamentals of inorganic glasses.* Amsterdam: Elsevier; 2019.
- Mauro J. Topological constraint theory of glass. *Am Ceram Soc Bull.* 2011;90:31–7.
- Pan Q, Ouyang T, Wu X, Huang X, Yang J, Kang S, et al. Emission color manipulation in transparent nanocrystals-in-glass composites fabricated by solution-combustion process. *Adv Opt Mater.* 2020;8(6):1901696.
- Gao G, Wei J, Shen Y, Peng M, Wondraczek L. Heavily Eu₂O₃-doped yttria-aluminoborate glasses for red photoconversion with a high quantum yield: luminescence quenching and statistics of cluster formation. *J Mater Chem C.* 2014;2(41):8678–82.
- Li G, Zhang C, Zhu P, Jiang C, Song P, Zhu K. Broadband near-infrared emission in Pr³⁺–Er³⁺ codoped phosphate glasses for optical amplifiers. *Ceram Int.* 2016;42(4):5558–61.
- Wondraczek L. Photoluminescence in glasses. *Encycl Glass Sci Technol Hist Cult.* 2021;1:693–703.
- Gao G, Meszaros R, Peng M, Wondraczek L. Broadband UV-to-green photoconversion in V-doped lithium zinc silicate glasses and glass ceramics. *Opt Express.* 2011;19(103):A312–8.
- Meng X, Tanaka K, Fujita K, Murai S. Intense greenish emission from d⁰ transition metal ion Ti⁴⁺ in oxide glass. *Appl Phys Lett.* 2007;90(5):051917.
- Guo H, Wei R, Liu X. Tunable white luminescence and energy transfer in (Cu⁺)₂, Eu³⁺ codoped sodium silicate glasses. *Opt Lett.* 2012;37(10):1670–72.
- Da N, Peng M, Krolikowski S, Wondraczek L. Intense red photoluminescence from Mn²⁺-doped (Na⁺; Zn²⁺) sulfophosphate

- glasses and glass ceramics as LED converters. *Opt Express*. 2010;18(3):2549–57.
17. Wang W, Yang X, Wieduwilt T, Schmidt MA, Zhang Q, Wondraczek L. Fluoride-sulfophosphate/silica hybrid fiber as a platform for optically active materials. *Front Mater*. 2019;6:148.
 18. Lin L, Wang Y, Lan B, Chen J, Lv S, Zhao Y, et al. Coordination geometry engineering in a doped disordered matrix for tunable optical response. *J Phys Chem C*. 2019;123(48):29343–52.
 19. Liu X, Zhou J, Zhou S, Yue Y, Qiu J. Transparent glass-ceramics functionalized by dispersed crystals. *Prog Mater Sci*. 2018;97:38–96.
 20. Wei R, Li J, Gao J, Guo H. Enhancement of Eu^{3+} luminescence by Ag species (Ag NPs, ML-Ag, Ag^+) in oxyfluoride glasses. *J Am Ceram Soc*. 2012;95(11):3380–2.
 21. Tanabe S, Feng X. Temperature variation of near-infrared emission from Cr^{4+} in aluminate glass for broadband telecommunication. *Appl Phys Lett*. 2000;77(6):818–20.
 22. Masai H, Fujiwara T, Matsumoto S, Tokuda Y, Yoko T. Emission property of Sn^{2+} -doped $\text{ZnO-P}_2\text{O}_5$ glass. *J Non-Cryst Solids*. 2014;383:184–7.
 23. Peng M, Dong G, Wondraczek L, Zhang L, Zhang N, Qiu J. Discussion on the origin of NIR emission from Bi-doped materials. *J Non-Cryst Solids*. 2011;357(11–13):2241–5.
 24. Peng M, Wondraczek L. Photoluminescence of $\text{Sr}_2\text{P}_2\text{O}_7$: Bi^{2+} as a red phosphor for additive light generation. *Opt Lett*. 2010;35(15):2544–6.
 25. Peng M, Da N, Krolikowski S, Stiegelschmitt A, Wondraczek L. Luminescence from Bi^{2+} -activated alkali earth borophosphates for white LEDs. *Opt Express*. 2009;17(23):21169–78.
 26. Masai H, Matsumoto S, Fujiwara T, Tokuda Y, Yoko T. Photoluminescent properties of Sb-doped phosphate glass. *J Am Ceram Soc*. 2012;95(3):862–65.
 27. Costa F, Souza A, Langaro A, Silva J, Santos F, Figueiredo M, et al. Observation of a Te^{4+} center with broad red emission band and high fluorescence quantum efficiency in $\text{TeO}_2\text{-Li}_2\text{O}$ glass. *J Lumin*. 2018;198:24–7.
 28. Reisfeld, R, Boehm, L, Barnett, B. Luminescence and nonradiative relaxation of Pb^{2+} , Sn^{2+} , Sb^{3+} , and Bi^{3+} in oxide glasses. *J Solid State Chem*. 1975;15(2):140–50.
 29. So, B, Heo, J, Liu, C, Ju, S, Han, W-T. Formation of channels containing lead sulfide quantum dots using continuous-wave laser for active planar waveguides in glasses. *Opt Mater Express*. 2017;7(1):281–5.
 30. Ueda, J, Hashimoto, A, Tanabe, S. Orange persistent luminescence and photodarkening related to paramagnetic defects of nondoped $\text{CaO-Ga}_2\text{O}_3\text{-GeO}_2$ glass. *J Phys Chem C*. 2019;123(49):29946–53.
 31. Zhou, S, Jiang, N, Zhu, B, Yang, H, Ye, S, Lakshminarayana, G, et al. Multifunctional bismuth-doped nanoporous silica glass: from blue-green, orange, red, and white light sources to ultra-broadband infrared amplifiers. *Adv Funct Mater*. 2008;18(9):1407–13.
 32. Bufetov I, Dianov E. Bi-doped fiber lasers. *Laser Phys Lett*. 2009;6(7):487.
 33. Fujimoto Y, Nakatsuka M. Infrared luminescence from bismuth-doped silica glass. *Jpn J Appl Phys*. 2001;40(3B):L279.
 34. Lu Z, Zhang W, Chen J, Chen S, Cao J, Guo H. Tunable photoemission and energy transfer of heavily Bi^{3+} , Eu^{3+} co-doped Y_4GeO_8 phosphors. *J Lumin*. 2021;232:117857.
 35. Zheng Z, Zhang J, Liu X, Wei R, Hu F, Guo H. Luminescence and self-referenced optical temperature sensing performance in $\text{Ca}_2\text{YZr}_2\text{Al}_3\text{O}_{12}$: Bi^{3+} , Eu^{3+} phosphors. *Ceram Int*. 2020;46(5):6154–9.
 36. Zhao Q, Hao Q, Luo Y, Peng G.-D. Thermal-induced luminescence enhancement of BAC-P in bismuth-doped phosphogermanosilicate fibers. *Opt Lett*. 2020;45(5):115–55.
 37. Cao J, Li L, Wang L, Li X, Zhang Z, Xu S, et al. Creating and stabilizing Bi NIR-emitting centers in low Bi content materials by topo-chemical reduction and tailoring of the local glass structure. *J Mater Chem C*. 2018;6(20):5384–90.
 38. Liu Y, Li J, Chen H, Sun L, Xu C. Enhanced broadband NIR emission of low Bi-doped borate glass by carbon reduction. *Mater Lett*. 2021;305:130791.
 39. Yang G, Chen D, Ren J, Xu Y, Zeng H, Yang Y, et al. Effects of melting temperature on the broadband infrared luminescence of Bi-doped and Bi/Dy co-doped chalcogenide glasses. *J Am Ceram Soc*. 2007;90(11):3670–2.
 40. Truong V, Bigot L, Lerouge A, Douay M, Razdobreev I. Study of thermal stability and luminescence quenching properties of bismuth-doped silicate glasses for fiber laser applications. *Appl Phys Lett*. 2008;92(4):041908.
 41. Firstov S, Firstova E, Alyshev S, Khopin V, Riumkin K, Melkumov M, et al. Recovery of IR luminescence in photo-bleached bismuth-doped fibers by thermal annealing. *Laser Phys*. 2016;26(8):084007.
 42. Peng M, Zhao Q, Qiu J, Wondraczek L. Generation of emission centers for broadband NIR luminescence in bismuthate glass by femtosecond laser irradiation. *J Am Ceram Soc*. 2009;92(2):542–44.
 43. Guo X, Li HJ, Su L, Yu P, Zhao H, Liu J, et al. Near-infrared broadband luminescence in $\text{Bi}_2\text{O}_3\text{-GeO}_2$ binary glass system. *Laser Phys*. 2011;21(5):901–05.
 44. Nielsen KH, Smedskjaer MM, Peng M, Yue Y, Wondraczek L. Surface-luminescence from thermally reduced bismuth-doped sodium aluminosilicate glasses. *J Non-Cryst Solids*. 2012;358(23):3193–9.
 45. Zhang Z, Cao J, Xue Y, Tan L, Xu S, Yang Z, et al. Tunable luminescence from bismuth-doped phosphate laser glass by engineering photonic glass structure. *J Am Ceram Soc*. 2018;101(5):1916–22.
 46. Li X, Cao J, Huang M, Peng M. Modulating broadband near infrared emission from Bi doped borate laser glass by codoping nonactive rare earth ions. *J Non-Cryst Solids*. 2021;553:120477.
 47. Peng J, Cao J, Tan L, Peng M. Glass-forming region and enhanced Bi NIR emission in sodium tantalum silicate laser glass. *J Am Ceram Soc*. 2019;102(5):2522–30.
 48. Liu C, Zhuang Y, Han J, Ruan J, Liu C, Zhao X. Multi-band near-infrared emission in low concentration bismuth doped alkaline earth alumino-boro-germanate glass. *Ceram Int*. 2020;46(10):15544–53.
 49. Romanov AN, Fattakhova ZT, Veber AA, Usovich OV, Haula EV, Korchak VN, et al. On the origin of near-IR luminescence in Bi-doped materials (II). Subvalent monocation Bi^+ and cluster Bi_5^{3+} luminescence in $\text{AlCl}_3/\text{ZnCl}_2/\text{BiCl}_3$ chloride glass. *Opt Express*. 2012;20(7):7212–20.
 50. Sun H, Zhou J, Qiu J. Recent advances in bismuth activated photonic materials. *Prog Mater Sci*. 2014;64:1–72.

51. Giraldo OG, Fei M, Wei R, Teng L, Zheng Z, Guo H. Energy transfer and white luminescence in Bi³⁺/Eu³⁺ co-doped oxide glasses. *J Lumin.* 2020;219:116918.
52. Dianov E. Nature of Bi-related near IR active centers in glasses: state of the art and first reliable results. *Laser Phys Lett.* 2015;12(9):095106.
53. Li X, Cao J, Xu W, Luo H, Wang Y, Wang X, et al. Photoemission from Bi-doped calcium aluminate glasses similar to sunlight. *J Am Ceram Soc.* 2019;102(5):2542–50.
54. Sellappan P, Rouxel T, Celarie F, Becker E, Houizot P, Conradt R. Composition dependence of indentation deformation and indentation cracking in glass. *Acta Mater.* 2013;61(16):5949–65.
55. Duffy JA. A common optical basicity scale for oxide and fluoride glasses. *J Non-Cryst Solids.* 1989;109(1):35–9.
56. Duffy JA. A review of optical basicity and its applications to oxidic systems. *Geochim Cosmochim Acta.* 1993;57(16):3961–70.
57. Inaba S, Fujino S, Morinaga K. Young's modulus and compositional parameters of oxide glasses. *J Am Ceram Soc.* 1999;82(12):3501–07.
58. Brüning R, Crowell T. A method to determine the kinetics of a supercooled liquid by temperature scanning measurements applied to (Li,Na)acetate and GeO₂. *J Non-Cryst Solids.* 1999;248(2):183–93.
59. Soga N. Pressure derivatives of the elastic constants of vitreous germania at 25°, –78.5°, and –195.8°C. *J Appl Phys.* 1969;40(8):3382–5.
60. Licheron M, Montouillout V, Millot F, Neuville DR. Raman and ²⁷Al NMR structure investigations of aluminate glasses: (1–x)Al₂O₃–xMO, with M = Ca, Sr, Ba and 0.5 < x < 0.75. *J Non-Cryst Solids.* 2011;357(15):2796–801.
61. McMILLAN P, Piriou B. Raman spectroscopy of calcium aluminate glasses and crystals. *J Non-Cryst Solids.* 1983;55(2):221–42.
62. Lin Y, Smedskjaer MM, Mauro JC. Structure, properties, and fabrication of calcium aluminate-based glasses. *Int J Appl Glass Sci.* 2019;10(4):488–501.
63. Henderson GS, Neuville DR, Cochain B, Cormier L. The structure of GeO₂–SiO₂ glasses and melts: a Raman spectroscopy study. *J Non-Cryst Solids.* 2009;355(8):468–74.
64. Santos LF, Wondraczek L, Deubener J, Almeida RM. Vibrational spectroscopy study of niobium germanosilicate glasses. *J Non-Cryst Solids.* 2007;353(18):1875–81.
65. Verweij H, Buster JHJM. The structure of lithium, sodium and potassium germanate glasses, studied by Raman scattering. *J Non-Cryst Solids.* 1979;34(1):81–99.
66. Di Martino D, Santos L, Marques A, Almeida R. Vibrational spectra and structure of alkali germanate glasses. *J Non-Cryst Solids.* 2001;293:394–401.
67. Tarte P. Infra-red spectra of inorganic aluminates and characteristic vibrational frequencies of AlO₄ tetrahedra and AlO₆ octahedra. *Spectrochim Acta A Mol Spectrosc.* 1967;23(7):2127–43.
68. Tarte P, Rulmont A, Liégeois-Duyckaerts M, Cahay R, Winand J. Vibrational spectroscopy and solid state chemistry. *Solid State Ionics.* 1990;42(3–4):177–96.
69. Li L, Cao J, Viana B, Xu S, Peng M. Site occupancy preference and antithermal quenching of the Bi²⁺ deep red emission in β-Ca₂P₂O₇: Bi²⁺. *Inorg Chem.* 2017;56(11):6499–506.
70. Liu X, Cheng C, Li X, Jiao Q, Dai S. Controllable ultra-broadband visible and near-infrared photoemissions in Bi-doped germanium-borate glasses. *J Am Ceram Soc.* 2020;103(1):183–92.
71. Güdel HU, Srivastava A, Brik M, Beers W, Cohen W. Reduced low temperature lifetimes of Bi³⁺ luminescence in magnetically ordered host lattices. *Opt Mater: X.* 2021;12:100094.
72. Wang L, Guo H, Wei Y, Noh HM, Jeong JH. White luminescence and energy transfer process in Bi³⁺, Sm³⁺ co-doped Ca₃Al₂O₆ phosphors. *Opt Mater.* 2015;42:233–6.
73. Jacquier B, Boulon G, Sallavaud G, Gaume-Mahn F. Bi³⁺ center in a lanthanum gallate phosphor. *J Solid State Chem.* 1972;4(3):374–8.
74. Bougon G, JC B. Spectroscopic properties of ³P₁ excited of Bi³⁺ in germinate glass. *Phys Rev B.* 1980;22:1163.
75. Peng M, Zollfrank C, Wondraczek L. Origin of broad NIR photoluminescence in bismuthate glass and Bi-doped glasses at room temperature. *J Phys: Condens Matter.* 2009;21(28):285106.
76. Quimby R, Shubochkin R, Morse T. High quantum efficiency of near-infrared emission in bismuth doped AlGeP-silica fiber. *Opt Lett.* 2009;34(20):3181–3.
77. Fujimoto YFY, Nakatsuka MNM. Infrared luminescence from bismuth-doped silica glass. *Jpn J Appl Phys.* 2001;40(3B):L279.
78. Ren J, Qiu J, Chen D, Hu X, Jiang X, Zhu C. Luminescence properties of bismuth-doped lime silicate glasses. *J Alloys Compd.* 2008;463(1–2):L5–8.
79. Murata T, Mouri T. Matrix effect on absorption and infrared fluorescence properties of Bi ions in oxide glasses. *J Non-Cryst Solids.* 2007;353(24–25):2403–07.
80. Khonthon S, Morimoto S, Arai Y, Ohishi Y. Redox equilibrium and NIR luminescence of Bi₂O₃-containing glasses. *Opt Mater.* 2009;31(8):1262–8.
81. Zheng J, Peng M, Kang F, Cao R, Ma Z, Dong G, et al. Broadband NIR luminescence from a new bismuth doped Ba₂B₅O₉Cl crystal: evidence for the Bi⁰ model. *Opt Express.* 2012;20(20):22569–78.
82. Peng M, Dong G, Wondraczek L, Zhang L, Zhang N, Qiu J. Discussion on the origin of NIR emission from Bi-doped materials. *J Non-Cryst Solids.* 2011;357(11):2241–5.
83. Sanz O, Haro-Poniatowski E, Gonzalo J, Fernández Navarro JM. Influence of the melting conditions of heavy metal oxide glasses containing bismuth oxide on their optical absorption. *J Non-Cryst Solids.* 2006;352(8):761–8.
84. Murata T, Torisaka M, Takebe H, Morinaga K. Compositional dependence of the valency state of Cr ions in oxide glasses. *J Non-Cryst Solids.* 1997;220(2–3):139–46.
85. Sokolov VO, Plotnichenko VG, Dianov EM. Origin of broadband near-infrared luminescence in bismuth-doped glasses. *Opt Lett.* 2008;33(13):1488–90.

How to cite this article: Cao J, Ding Y, Limbach R, Nozari V, Sajzew R, Sun M, et al. Tunable broadband photoluminescence from bismuth-doped calcium aluminum germanate glasses prepared in oxidizing atmosphere. *J Am Ceram Soc.* 2022;105:5676–5686.
<https://doi.org/10.1111/jace.18513>